Available online at www.sciencedirect.com
ScienceDirect
Journal of Computational Physics 226 (2007) 244–262
JOURNAL OF COMPUTATIONAL PHYSICS
www.elsevier.com/locate/jcp

New conservative gyrokinetic full-f Vlasov code and its comparison to gyrokinetic δf particle-in-cell code

Yasuhiro Idomura [a,*], Masato Ida [a], Shinji Tokuda [a], Laurent Villard [b]

[a] Japan Atomic Energy Agency, Higashi-Ueno 6-9-3, Taitou, Tokyo 110-0015, Japan
[b] Centre de Recherches en Physique des Plasmas, Ecole Polytechnique Fédérale de Lausanne, Euratom-Suisse, 1015 Lausanne, Switzerland

Received 10 June 2006; received in revised form 26 January 2007; accepted 6 April 2007
Available online 24 April 2007

Abstract

A new conservative gyrokinetic full-f Vlasov code is developed using a finite difference operator which conserves both the $L1$ and $L2$ norms. The growth of numerical oscillations is suppressed by conserving the $L2$ norm, and the code is numerically stable and robust in a long time simulation. In the slab ion temperature gradient driven (ITG) turbulence simulation, the energy conservation and the entropy balance relation are confirmed, and solutions are benchmarked against a conventional δf particle-in-cell (PIC) code. The results show that the exact particle number conservation and the good energy conservation in the conservative Vlasov simulation are advantageous for a long time micro-turbulence simulation. In the comparison, physical and numerical effects of the $v_\parallel$ nonlinearity are clarified for the Vlasov and PIC simulations.

Keywords: Gyrokinetic equation; Vlasov simulation; Particle-in-cell simulation; Conservative schemes; Fusion plasmas; Long time micro-turbulence simulations

1. Introduction

Five dimensional (5D) gyrokinetic simulations are essential tools to study anomalous turbulent transport in tokamak plasmas [1–3]. Although several gyrokinetic simulations have been developed based on particle (Lagrangian) and mesh (Eulerian) approaches, most of full torus global simulations have adopted a particle approach [4–8] because of limitations on computational resources such as the memory size. A δf particle-in-cell (PIC) method [9–11] enabled an accurate calculation of small amplitude turbulent fluctuations with $\delta n/n_0 \sim 1\%$ in a collisionless fusion plasma, where n_0 and δn are the equilibrium and fluctuating density. However, the method is based on the conservation property or the Liouville's theorem in a collisionless gyrokinetic equation, and in a broad sense, most of the δf PIC simulations are decaying turbulence simulations, where an isolated system without collisions and sources is relaxed from a linearly unstable initial condition to a nonlinearly saturated state. Starting from early pioneering works [4–6], such decaying turbulence simulations played

* Corresponding author.
E-mail address: idomura.yasuhiro@jaea.go.jp (Y. Idomura).

0021-9991/$ - see front matter
doi:10.1016/j.jcp.2007.04.013

significant roles in studying physical issues behind tokamak turbulent transport. For example, recent works addressed nonlinear processes leading to structure formations such as the magnetic shear dependence of the electron temperature gradient driven (ETG) turbulence [12], the self-organisation of ETG zonal flows [13], and the plasma current dependence of zonal flows and geodesic acoustic modes in the ion temperature gradient driven (ITG) turbulence [14]. Although decaying turbulence simulations of collisionless and sourceless system are still useful for studying transient nonlinear processes coming from the Hamiltonian dynamics, from the viewpoint of the entropy balance relation [15–17], they do not reach at statistically steady states until the heat transport is almost quenched by stabilising effects such as zonal flows and quasi-linear flattening [18]. Such simulations are also characterised by strong profile relaxations due to linear modes, and therefore their relaxed states are not the same as those would be attained if real collisions, sources, and sinks were included. In this sense, the existing decaying turbulence simulations are not enough for estimating realistic turbulent transport coefficients for quasi-steady equilibrium profiles balanced with real sources. In addition, more realistic long time turbulence simulations with collisions and sources are desirable to address future issues, for example, the formation of transport barriers. Extensions of the δf method have been attempted for a driven local system [19], a heat source model [20], and a collisional effect [21]. However, Ref. [22] showed that complicated statistical treatments are needed to define δf in the system with non-conservative effects, where nonlinear characteristics cross each other. Although the collisional δf method based on this approach was successfully applied to neoclassical δf simulations [23,24], further developments are needed before applying it to tokamak microturbulence.

On the other hand, a mesh approach, which is often called Vlasov or continuum, is much more flexible in treating these non-conservative effects, and is likely to become another solution because of recent advances in computational fluid dynamics (CFD) schemes and increasing computational resources. So far, local flux tube toroidal δf simulations [25–27] and its extension including global profile effects [28] were developed with spectral and dissipative finite difference methods. Although a δf approach, in which local background gradients are fixed on average, may be useful for estimating quasi-steady transport coefficients for given density and temperature profiles, such a fixed gradient assumption may not be valid for studying fast time scale ($\sim$ms) profile variations such as avalanche like phenomena [29] and transient changes of profiles and turbulent transport in the modulation experiments [30]. Moreover, turbulent time scale relaxation oscillation events such as bursts and avalanches were reported in flux driven fluid simulations [31,32]. A global full-f approach with evolving background profiles is desirable in studying interactions between transient turbulent transport and profile formations, which dictate intermittent behaviours of turbulent transport and formations of transport barriers. As for a global full-f approach, cylindrical [33,34] and slab [35] gyrokinetic Vlasov codes were developed using the semi-Lagrangian method [36] and the constrained-interpolation-profile (CIP) method [37], and they were benchmarked against PIC codes. However, in our previous work [35], the quality of the energy and particle number conservations in the Vlasov CIP code was almost the same level as in the δf PIC code, and the breakdown of conservation properties was still problematic in a long time micro-turbulence simulation. To resolve this issue, we need a conservative full-f Vlasov code that is numerically stable and robust in a long time micro-turbulence simulation.

In contrast to the Vlasov–Poisson system, the Hamiltonian of the toroidal gyrokinetic Vlasov–Poisson system is not separable because of $E \times B$ and magnetic drifts, and the splitting method [41], which is sort of second-order symplectic integration, is not available. Therefore, a direct treatment of incompressible Hamiltonian flows in 5D phase space is required to develop a conservative gyrokinetic simulation. Although several semi-Lagrangian type conservative methods have been proposed [38–40], their extension to multiple dimension without the splitting method may be costly because of high dimensional interpolation. As for a conventional Eulerian scheme, a finite volume method or a centred finite difference method conserves the particle distribution function, F, but the scheme often becomes unstable when numerical oscillations due to aliasing errors are produced. The aliasing error is inevitable in resolving fine scale structures or filamentation with finite discrete grids. However, in Ref. [42], it was pointed out that such a numerical instability may be avoided by conserving the square quantity, which bounds the amplitude of numerical oscillations. Morinishi et al. proposed a new finite difference operator, which can be easily extended to higher order accuracy and conserves both the momentum and kinetic energy, which correspond to F and F^2 in the present problem, and it was successfully applied to incompressible neutral fluid simulations [43]. An importance of the conservations of F and

F^2 was pointed out also in recent gyrokinetic Vlasov simulations [44,28]. It may also be possible to avoid numerical oscillations using non-oscillatory advection schemes such as total variation diminishing (TVD) type schemes, which make use of numerical dissipation. However, in the present problem, the Morinishi scheme is preferable, because its concept naturally fits the first principles of the gyrokinetic equation, which conserves F and F^2 as the Casimir invariants.

In this work, we develop a conservative Gyrokinetic 5D full-f Vlasov code (G5D) using the Morinishi scheme, and discuss its numerical properties by comparing the results from ITG turbulence simulations with the Morinishi scheme and with a finite volume method. We then show benchmarks of ITG turbulence simulations between the new Vlasov code and a conventional δf PIC code, and discuss a possibility of a long time micro-turbulence simulation.

As an application of the new Vlasov code to a physical problem, we study a role of the $v_\parallel$ nonlinearity. In the gyrokinetic simulation, the $v_\parallel$ nonlinearity is often ignored, because this term is one of higher order effects according to the gyrokinetic ordering. Historically, the gyrokinetic equation based on the recursive method [45] was formulated without this term, and the equation is still used in several gyrokinetic simulations. In Ref. [46], it was reported that in cylindrical simulations of ITG turbulence, not only particle noise but also neglecting the $v_\parallel$ nonlinearity affect the error on the particle number conservation, leading to erroneous zonal flow structures and thereby potentially affecting the computed level of heat transport. However, in slab or cylindrical models, the $v_\parallel$ nonlinearity itself does not violate the particle number conservation, and it is not clear whether the effect is numerical or physical. In the present study, we discuss numerical effects of the $v_\parallel$ nonlinearity on the Vlasov and PIC simulations, and then validate its physical effects by showing the entropy balance relation. Exact conservation properties of the new Vlasov code are useful in distinguishing numerical from physical effects.

The reminder of the paper is organised as follows. In Section 2, we describe a 5D gyrokinetic model and its reduced 4D model, and show conservation properties in these models. In Section 3, we present the Morinishi scheme and its application to the gyrokinetic model. In Section 4, we discuss numerical properties of the new conservative gyrokinetic full-f Vlasov code by comparing 4D ITG turbulence simulations with the Morinishi scheme and with a finite volume method. In Section 5, we give benchmarks of 4D and 5D ITG turbulence simulations between the new Vlasov code and a conventional PIC code. In the comparison, we also clarify numerical and physical effects of the $v_\parallel$ nonlinearity on the Vlasov and PIC simulations. Finally, a summary is given in Section 6.

2. Calculation model

In the present study, we consider the electrostatic ITG turbulence described by gyrokinetic ions and adiabatic electrons in a slab configuration with a uniform equilibrium magnetic field, $\mathbf{B} = B_0\mathbf{b}$, where $\mathbf{b}$ is the unit vector in the direction of the magnetic field. In the modern gyrokinetic theory [47], the gyrokinetic equation is written using the gyro-averaged Hamiltonian H in the gyrocenter coordinates, $\mathbf{Z} = (t; \mathbf{R}, v_\parallel, \mu, \alpha)$,

$$H = \frac{1}{2} m_i v_\parallel^2 + \mu B_0 + q_i \langle \phi \rangle_\alpha, \tag{1}$$

where $\mathbf{R}$ is a position of the guiding centre, $v_\parallel$ is the parallel velocity, μ is the magnetic moment, α is the gyrophase angle, m_s and q_s are the mass and charge of the particle species s, respectively, ϕ is the electrostatic potential, and the gyro-averaging operator is defined as $\langle \cdot \rangle_\alpha \equiv \oint \cdot \, \mathrm{d}\alpha/2\pi$. This Hamiltonian yields the gyrokinetic equation,

$$\frac{\mathrm{D}F}{\mathrm{D}t} \equiv \frac{\partial F}{\partial t} + \{F, H\} = \frac{\partial F}{\partial t} + \{\mathbf{R}, H\} \cdot \frac{\partial F}{\partial \mathbf{R}} + \{v_\parallel, H\} \frac{\partial F}{\partial v_\parallel} = 0, \tag{2}$$

and its nonlinear characteristics,

$$\frac{\mathrm{d}\mathbf{R}}{\mathrm{d}t} \equiv \{\mathbf{R}, H\} = v_\parallel \mathbf{b} + \frac{c}{B_0} \mathbf{b} \times \nabla \langle \phi \rangle_\alpha, \tag{3}$$

$$\frac{\mathrm{d}v_\parallel}{\mathrm{d}t} \equiv \{v_\parallel, H\} = -\frac{q_i}{m_i} \mathbf{b} \cdot \nabla \langle \phi \rangle_\alpha, \tag{4}$$

where $\{\cdot,\cdot\}$ is the Poisson bracket in the gyrocenter coordinates, F is the guiding centre distribution function, and c is the velocity of light. In the configuration space, we use Cartesian coordinates, (x, y, z), where the field is imposed in the z direction, $\mathbf{b} = \mathbf{e}_z$, the system is periodic in the y and z directions, and equilibrium quantities vary in the x direction. The equilibrium distribution function, F_0, is given by a local Maxwellian distribution function,

$$F_0(x, v_\parallel, \mu) = f_0(x, v_\parallel) g_0(x, \mu), \tag{5}$$

$$f_0(x, v_\parallel) = \frac{n_0(x)}{(2\pi m_i T_{i0}(x))^{1/2}} \exp\left(-\frac{m_i v_\parallel^2/2}{T_{i0}(x)}\right), \tag{6}$$

$$g_0(x, \mu) = \frac{1}{2\pi m_i T_{i0}(x)} \exp\left(-\frac{\mu B_0}{T_{i0}(x)}\right), \tag{7}$$

where n_0 and T_{i0} are the equilibrium density and temperature, respectively. The electrostatic potential ϕ is determined by the gyrokinetic Poisson equation,

$$-\left(\nabla^2 + \frac{\rho_{\mathrm{ti}}^2}{\lambda_{\mathrm{Di}}^2}\nabla_\perp^2\right)\phi + \frac{1}{\lambda_{\mathrm{De}}^2}(\phi - \langle\phi\rangle_{\mathrm{f}}) = 4\pi\left[q_{\mathrm{i}}\int \delta F \delta([\mathbf{R} + \boldsymbol{\rho}] - \mathbf{x})\, \mathrm{d}^6 Z - q_{\mathrm{e}}\delta n_{0e}\right], \tag{8}$$

where $\delta F = F - F_0$, δn_{0e} is the initial perturbation given for the electron density, $\mathrm{d}^6 Z = m_i^2 B_0\, \mathrm{d}\mathbf{R}\, \mathrm{d}v_\parallel\, \mathrm{d}\mu\, \mathrm{d}\alpha$, $\nabla_\perp = \partial_x \mathbf{e}_x + \partial_y \mathbf{e}_y$, ρ_{ti} is the ion Larmor radius, λ_{De} and λ_{Di} are the electron and ion Debye lengths. In the present study, the adiabatic electron response is defined using the electrostatic potential averaged over the constant pressure surface or the y–z surface, $\langle\phi\rangle_{\mathrm{f}} \equiv \int \phi\, \mathrm{d}y\, \mathrm{d}z/(L_y L_z)$, where L_x, L_y, and L_z are the system size in the x, y, and z directions, respectively.

Eq. (2) is the Liouville equation, which shows that F is conserved along the nonlinear characteristics. This also leads to a conservation of an arbitrary function, $C(F)$, along the nonlinear characteristics,

$$\frac{\mathrm{D}C(F)}{\mathrm{D}t} \equiv \frac{\partial C(F)}{\partial t} + \{C(F), H\} = 0. \tag{9}$$

Therefore, in addition to the total particle number or the $L1$ norm, $N = \int F\, \mathrm{d}^6 Z$, the system has an infinite number of conserved quantities such as the $L2$ norm, $M = \int F^2\, \mathrm{d}^6 Z$, and the kinetic entropy, $S = -\int F \ln F\, \mathrm{d}^6 Z$. From the viewpoints of the accuracy and stability of a conservative Vlasov simulation, conservations of the $L1$ and $L2$ norms are particularly important. Another physically relevant conservation property is the total energy conservation,

$$\int H \frac{\partial F}{\partial t}\, \mathrm{d}^6 Z = \frac{\mathrm{d}E_{\mathrm{k}}}{\mathrm{d}t} + \frac{\mathrm{d}E_{\mathrm{f}}}{\mathrm{d}t} = 0, \tag{10}$$

$$\frac{\mathrm{d}E_{\mathrm{k}}}{\mathrm{d}t} = \frac{\mathrm{d}}{\mathrm{d}t}\int \left(\frac{1}{2} m_i v_\parallel^2 + \mu B_0\right) F\, \mathrm{d}^6 Z, \tag{11}$$

$$\frac{\mathrm{d}E_{\mathrm{f}}}{\mathrm{d}t} = \int q_i \langle\phi\rangle_\alpha \frac{\partial F}{\partial t}\, \mathrm{d}^6 Z = \frac{\mathrm{d}}{\mathrm{d}t}\frac{1}{8\pi}\int \left[|\nabla\phi|^2 + \frac{\rho_{\mathrm{ti}}^2}{\lambda_{\mathrm{Di}}^2}|\nabla_\perp\phi|^2 + \frac{1}{\lambda_{\mathrm{De}}^2}|\phi - \langle\phi\rangle_{\mathrm{f}}|^2\right] \mathrm{d}x\, \mathrm{d}y\, \mathrm{d}z. \tag{12}$$

In the limiting case without gyro-averaging or $\langle\phi\rangle_\alpha \to \phi$, the μ dependence of F can be assumed to be a local Maxwellian distribution, $F(\mathbf{R}, v_\parallel, \mu) = f(\mathbf{R}, v_\parallel) g_0(x, \mu)$. By integrating F over μ, the gyrokinetic Vlasov–Poisson system, (2)–(8), yields a reduced model consisting of the 4D drift-kinetic equation,

$$h = \frac{1}{2} m_i v_\parallel^2 + \mu B_0 + q_i \phi, \tag{13}$$

$$\frac{\mathrm{D}f}{\mathrm{D}t} \equiv \frac{\partial f}{\partial t} + \{f, h\} = \frac{\partial f}{\partial t} - \frac{c}{B_0}\frac{\partial\phi}{\partial y}\frac{\partial f}{\partial x} + \frac{c}{B_0}\frac{\partial\phi}{\partial x}\frac{\partial f}{\partial y} + v_\parallel \frac{\partial f}{\partial z} - \frac{q_i}{m_i}\frac{\partial\phi}{\partial z}\frac{\partial f}{\partial v_\parallel} = 0, \tag{14}$$

and the gyrokinetic Poisson equation,

$$-\left(\nabla^2 + \frac{\rho_{\mathrm{ti}}^2}{\lambda_{\mathrm{Di}}^2}\nabla_\perp^2\right)\phi + \frac{1}{\lambda_{\mathrm{De}}^2}(\phi - \langle\phi\rangle_{\mathrm{f}}) = 4\pi\left[q_{\mathrm{i}}\int \delta f m_i\, \mathrm{d}v_\parallel - q_{\mathrm{e}}\delta n_{0e}\right], \tag{15}$$

where the finite Larmor radius (FLR) effect is kept only in the ion polarisation density (the second term in the l.h.s. of Eq. (15)). The conservation properties are derived in a similar way as in the 5D gyrokinetic Vlasov–Poisson system. In order to save computational cost, we use the 4D model to discuss the numerical properties of the new Vlasov code.

3. $L1$ and $L2$ Conservative finite difference operator

The drift-kinetic equation (14) may be written as

$$\frac{\partial f}{\partial t} + v_j \frac{\partial f}{\partial x_j} = 0, \tag{16}$$

where v_j are the nonlinear characteristics, x_j are variables in the gyrocenter coordinates, and the index j runs through $j = 1$–4. It is noted that the 5D gyrokinetic equation can also be written in the same form, because μ is a constant of motion and enters parametrically in the gyrokinetic equation. Discussions in this section are applicable also to Eq. (2). The nonlinear characteristics are given by Hamilton's equation, $v_j \equiv \{x_j, h\}$, which satisfy

$$\frac{\partial v_j}{\partial x_j} = 0. \tag{17}$$

Therefore, the problem is seen as the continuity equation for f transported by incompressible Hamiltonian flows in phase space. In order to discuss conservation properties in this problem, we introduce symbolic notations following Ref. [43],

$$\frac{\partial f}{\partial t} + (\text{Conv.}) = 0. \tag{18}$$

The operator (Conv.) may be written in the following three types of convective forms, the divergence form, (Div.), the advection form, (Adv.), and the skew-symmetric form, (Skew.),

$$(\text{Div.}) \equiv \frac{\partial v_j f}{\partial x_j}, \tag{19}$$

$$(\text{Adv.}) \equiv v_j \frac{\partial f}{\partial x_j} = (\text{Div.}) - f(\text{Cont.}), \tag{20}$$

$$(\text{Skew.}) \equiv \frac{1}{2}\frac{\partial v_j f}{\partial x_j} + \frac{1}{2} v_j \frac{\partial f}{\partial x_j} = (\text{Div.}) - \frac{1}{2} f(\text{Cont.}), \tag{21}$$

where

$$(\text{Cont.}) \equiv \frac{\partial v_j}{\partial x_j}. \tag{22}$$

(Div.) trivially conserves the total particle number or the $L1$ norm, while (Adv.) and (Skew.) conserve it provided that the flow is exactly solenoidal or (Cont.) $= 0$. By multiplying f, Eq. (18) yields the continuity equation for $f^2/2$,

$$\frac{\partial f^2/2}{\partial t} + f(\text{Conv.}) = 0. \tag{23}$$

f(Conv.) can also be written using the above three operators,

$$f(\text{Div.}) = \frac{\partial v_j f^2/2}{\partial x_j} + \frac{1}{2} f^2(\text{Cont.}), \tag{24}$$

$$f(\text{Adv.}) = \frac{\partial v_j f^2/2}{\partial x_j} - \frac{1}{2} f^2(\text{Cont.}), \tag{25}$$

$$f(\text{Skew.}) = \frac{\partial v_j f^2/2}{\partial x_j}. \tag{26}$$

In contrast to the $L1$ norm, the $L2$ norm is trivially conserved with (Skew.), while (Div.) and (Adv.) are conservative for the $L2$ norm when (Cont.) $= 0$.

We then discuss conservation properties of the $L1$ and $L2$ norms for discrete operators. In the present work, we use a uniform regular grid system where both f and v_j are defined at the same grid points. We use the following notations in writing discrete operators,

$$\frac{\delta_n A}{\delta_n x_1} \equiv \frac{A(x_1 + nh_1/2, x_2, x_3, x_4) - A(x_1 - nh_1/2, x_2, x_3, x_4)}{nh_1}, \tag{27}$$

$$\bar{A}^{nx_1} \equiv \frac{1}{2}A(x_1 + nh_1/2, x_2, x_3, x_4) + \frac{1}{2}A(x_1 - nh_1/2, x_2, x_3, x_4), \tag{28}$$

$$\widetilde{AB}^{nx_1} \equiv \frac{1}{2}A(x_1 + nh_1/2, x_2, x_3, x_4)B(x_1 - nh_1/2, x_2, x_3, x_4) + \frac{1}{2}A(x_1 - nh_1/2, x_2, x_3, x_4)B(x_1 + nh_1/2, x_2, x_3, x_4), \tag{29}$$

where h_j is the grid spacing in the x_j direction and n is an integer. It is noted that only in Eqs. (27)–(29), we use n differently from the other equations. By applying a second-order accurate centred finite difference to Eqs. (19)–(21), we have the following convective operators:

$$[\text{Div.}] \equiv \frac{\delta_2 v_j f}{\delta_2 x_j}, \tag{30}$$

$$[\text{Adv.}] \equiv v_j \frac{\delta_2 f}{\delta_2 x_j} = \frac{\delta_1 \widetilde{v_j f}^{1x_j}}{\delta_1 x_j} - f[\text{Cont.}], \tag{31}$$

$$[\text{Skew.}] \equiv \frac{1}{2}[\text{Div.}] + \frac{1}{2}[\text{Adv.}] = \frac{\delta_1 \bar{v}_j^{1x_j} \bar{f}^{1x_j}}{\delta_1 x_j} - \frac{1}{2} f[\text{Cont.}], \tag{32}$$

where

$$[\text{Cont.}] \equiv \frac{\delta_2 v_j}{\delta_2 x_j}. \tag{33}$$

The $L1$ norm is automatically conserved by [Div.], which is equivalent to a finite volume method or a centred finite difference method. On the other hand, [Adv.] and [Skew.] conserve the $L1$ norm if v_j is discretised so that [Cont.] $= 0$ is satisfied. The conservation property of the $L2$ norm is seen by discrete forms of Eqs. (24)–(26),

$$f[\text{Div.}] = \frac{\delta_1 f\widetilde{(v_j f)}^{1x_j}}{\delta_1 x_j} - v_j f \frac{\delta_2 f}{\delta_2 x_j}, \tag{34}$$

$$f[\text{Skew.}] = \frac{\delta_1 \bar{v}_j^{1x_j} \widetilde{f^2/2}^{1x_j}}{\delta_1 x_j}, \tag{35}$$

$$f[\text{Adv.}] = 2f[\text{Skew.}] - f[\text{Div.}]. \tag{36}$$

Here, the $L2$ norm is conserved only with [Skew.].

As mentioned above, discretised forms of the nonlinear characteristics dictate the conservation properties of the discrete operator. In the present 4D model, we define v_j as

$$v_1 = -\frac{c}{B_0}\frac{\delta_2 \phi}{\delta_2 y}, \tag{37}$$

$$v_2 = \frac{c}{B_0}\frac{\delta_2 \phi}{\delta_2 x}, \tag{38}$$

$$v_3 = v_\parallel, \tag{39}$$

$$v_4 = -\frac{q_i}{m_i}\frac{\delta_2 \phi}{\delta_2 z}, \tag{40}$$

where ϕ is determined self-consistently by solving the gyrokinetic Poisson equation (15). Since Eqs. (37)–(40) definitely satisfy $[\text{Cont.}] = 0$, the skew-symmetric operator conserves both the $L1$ and $L2$ norms. However, precisely speaking, the conservation of the $L2$ norm depends also on the time integration scheme. If one uses non-dissipative methods such as the implicit midpoint rule or its higher order extensions [48,49,44], the $L2$ norm may be exactly conserved. But, such an implicit scheme is costly, especially for the 5D gyrokinetic simulation. In the present study, we use the fourth-order Runge–Kutta method which leads to a small error in the $L2$ norm conservation by weak numerical dissipation.

A fourth-order accurate convective operator, $\langle\text{Skew.}\rangle$, is obtained as a combination of the second-order accurate convective operator, [43]

$$\langle\text{Skew.}\rangle \equiv \frac{4}{3}\frac{\delta_1 \bar{v}_j^{1x_j} \bar{f}^{1x_j}}{\delta_1 x_j} - \frac{1}{3}\frac{\delta_2 \bar{v}_j^{2x_j} \bar{f}^{2x_j}}{\delta_2 x_j} - f\frac{1}{2}\langle\text{Cont.}\rangle, \tag{41}$$

$$f\langle\text{Skew.}\rangle = \frac{4}{3}\frac{\delta_1 \bar{v}_j^{1x_j} \widetilde{f^2/2}^{1x_j}}{\delta_1 x_j} - \frac{1}{3}\frac{\delta_2 \bar{v}_j^{2x_j} \widetilde{f^2/2}^{2x_j}}{\delta_2 x_j}, \tag{42}$$

$$\langle\text{Cont.}\rangle \equiv \frac{4}{3}\frac{\delta_2 v_j}{\delta_2 x_j} - \frac{1}{3}\frac{\delta_4 v_j}{\delta_4 x_j}. \tag{43}$$

The corresponding definitions of v_j are given as

$$v_1 = -\frac{c}{B_0}\left[\frac{4}{3}\frac{\delta_2\phi}{\delta_2 y} - \frac{1}{3}\frac{\delta_4\phi}{\delta_4 y}\right], \tag{44}$$

$$v_2 = \frac{c}{B_0}\left[\frac{4}{3}\frac{\delta_2\phi}{\delta_2 x} - \frac{1}{3}\frac{\delta_4\phi}{\delta_4 x}\right], \tag{45}$$

$$v_3 = v_\parallel, \tag{46}$$

$$v_4 = -\frac{q_i}{m_i}\left[\frac{4}{3}\frac{\delta_2\phi}{\delta_2 z} - \frac{1}{3}\frac{\delta_4\phi}{\delta_4 z}\right]. \tag{47}$$

These definitions satisfy $\langle\text{Cont.}\rangle = 0$, and both the $L1$ and $L2$ norms are conserved with $\langle\text{Skew.}\rangle$. This operator is applicable also to the 5D gyrokinetic model by replacing ϕ with $\langle\phi\rangle_\alpha$.

4. Numerical properties of new Vlasov code

In studying numerical properties of the new Vlasov code, we solve the ITG turbulence using a reduced 4D model without the gyro-averaging. The drift-kinetic equation (14) is discretised using the second-order accurate skew-symmetric finite difference operator (32). The time integration is performed with the fourth-order Runge–Kutta method with an adaptive control of the time step width which keeps the CFL (Courant–Friedrichs–Lewy) number, τ, constant. The gyrokinetic Poisson equation is solved using a fast Fourier transform (FFT) technique. A finite difference solver and a FFT solver are parallelised with 2D domain decomposition (x–y or k_x–k_y), and all the communications are implemented using the MPI2 put/get. In the 5D gyrokinetic simulation, where μ appears in the gyro-averaging operator, the code is parallelised also in the μ direction. We write the gyro-averaging operator in Fourier space,

$$\phi(\mathbf{x},t) = \sum_{\mathbf{k}} \phi_{\mathbf{k}}(t) e^{i\mathbf{k}\cdot\mathbf{x}}, \tag{48}$$

$$\langle\phi(\mathbf{R},t)\rangle_\alpha = \sum_{\mathbf{k}} \phi_{\mathbf{k}}(t) J_0(k_\perp\rho) e^{i\mathbf{k}\cdot\mathbf{R}}, \tag{49}$$

$$\delta F(\mathbf{R}, v_\parallel, \mu, t) = \sum_{\mathbf{k}} \delta F_{\mathbf{k}}(v_\parallel, \mu, t) e^{i\mathbf{k}\cdot\mathbf{R}}, \tag{50}$$

$$\int \delta F \delta([\mathbf{R}+\boldsymbol{\rho}] - \mathbf{x})\, d^6Z = \sum_{\mathbf{k}} 2\pi \int \delta F_{\mathbf{k}}(v_\parallel, \mu, t) J_0(k_\perp\rho) e^{i\mathbf{k}\cdot\mathbf{x}} m_i^2 B_0 dv_\parallel d\mu, \tag{51}$$

where $J_0(k_\perp\rho)$ is the zeroth-order Bessel function, $\rho = v_\perp/\Omega_i$, $v_\perp = \sqrt{2\mu B_0/m_i}$, and $\Omega_i = q_i B_0/m_i c$. Since μ enters the gyrokinetic equation parametrically, the code is designed as a cluster of 4D simulations with different gyro-averaging operators, which are coupled through the gyrokinetic Poisson equation (8). Communications among different μ parts are implemented using the MPI1 group communication. Fig. 1 shows the performance evaluation of the new Vlasov code on the JAEA (Japan Atomic Energy Agency) Altix3700Bx2 system, which consists of 2048 processing elements with the total performance of 13Tflops and the total memory size of 13TB, where each processing element has an Itanium2 processor (1.6 GHz, 6.4 Gflops) with 6.4GB memory. In Fig. 1a, the processor number scan with fixed problem size ($N_x \times N_y \times N_z \times N_{v_\parallel} \times N_\mu = 512 \times 512 \times 64 \times 100 \times 24$, ~2TB memory) shows degradation of the sustained performance from ~26.4% with 384 processors to ~18.2% with 1536 processors. In Fig. 1b, the ratio of the processing speed of 1536 processors to 384 processors is ~2.7. On the other hand, the processor number scan with scaling problem size ($N_x \times N_y \times N_z \times N_{v_\parallel} \times N_\mu = 512 \times 512 \times 64 \times 100 \times 24$, ~2TB memory for 384 processors, $N_x \times N_y \times N_z \times N_{v_\parallel} \times N_\mu = 512 \times 512 \times 64 \times 100 \times 48$, ~4TB memory for 768 processors, and $N_x \times N_y \times N_z \times N_{v_\parallel} \times N_\mu = 512 \times 512 \times 64 \times 100 \times 96$, ~8TB memory for 1536 processors) does not show such degradation and the sustained performance is kept around ~25%.

In the present 4D simulation, we consider a hydrogen plasma in a slab configuration with $L_x = 2L_y \sim 32\rho_{\rm ti}$, $L_z \sim 8000\rho_{\rm ti}$, and $L_{v_\parallel} = 10v_{\rm ti}$ ($v_\parallel = -5v_{\rm ti} \sim 5v_{\rm ti}$). n_0 and T_{e0} are assumed to be homogeneous, and T_{i0} is given as

$$T_{i0}(x) = \bar{T}_i\left[1 - \frac{L_x}{2\pi L_{\rm ti}}\cos\frac{2\pi x}{L_x}\right], \tag{52}$$

where $\bar{T}_i = T_{e0}$ and $L_{\rm ti} \sim 37\rho_{\rm ti}$ (see Fig. 2a). In the equilibrium profile (52), positive and negative temperature gradient regions coexist so that we can use the periodic boundary condition also in the x direction. The boundary condition in the $v_\parallel$ direction is given as $\bar{v}_4^{1x_4} = 0$ at the boundary. This boundary condition does not affect the conservations of the $L1$ and $L2$ norms. The initial condition is given by a local Maxwellian distribution, f_0, for ions, and a small initial perturbation with the Gaussian distribution is given for the electron density,

$$\delta n_{0e} = n_0\epsilon_0 \exp\left[-\frac{(x/L_x - 1/2)^2 + (y/L_y - 1/2)^2 + (z/L_z - 1/2)^2}{2\sigma^2}\right], \tag{53}$$

where we use $\epsilon_0 = 10^{-10}$ and $\sigma = 0.1$. From a convergence study, we have determined numerical parameters of the standard case with the grid number, $N_x \times N_y \times N_z \times N_{v_\parallel} = 128 \times 64 \times 32 \times 128$ ($\Delta x = \Delta y \sim \rho_{\rm ti}/4$), and the CFL number, $\tau = 0.4$, which corresponds to $\Delta t \sim 20\Omega_i^{-1}$ and $\Delta t \sim 7\Omega_i^{-1}$ in the linear and nonlinear phases, respectively. Since the present simulation has neither a collision term nor any other dissipation models to

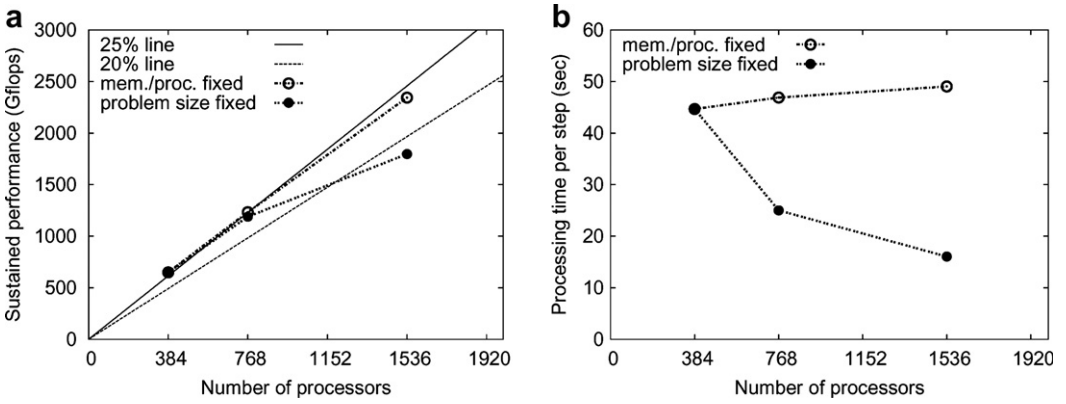

Fig. 1. Parallel processing performances of G5D code on the JAEA Altix3700B × 2 system. (a) and (b) shows the sustained performance and the processing time of a single step with different numbers of processors. The cases with fixed problem size ($N_x \times N_y \times N_z \times N_{v_\parallel} \times N_\mu = 512 \times 512 \times 64 \times 100 \times 24$, ~2TB memory) and with scaling problem size ($N_x \times N_y \times N_z \times N_{v_\parallel} \times N_\mu = 512 \times 512 \times 64 \times 100 \times 24$, ~2TB memory for 384 processors, $N_x \times N_y \times N_z \times N_{v_\parallel} \times N_\mu = 512 \times 512 \times 64 \times 100 \times 48$, ~4TB memory for 768 processors, and $N_x \times N_y \times N_z \times N_{v_\parallel} \times N_\mu = 512 \times 512 \times 64 \times 100 \times 96$, ~8TB memory for 1536 processors) are plotted.

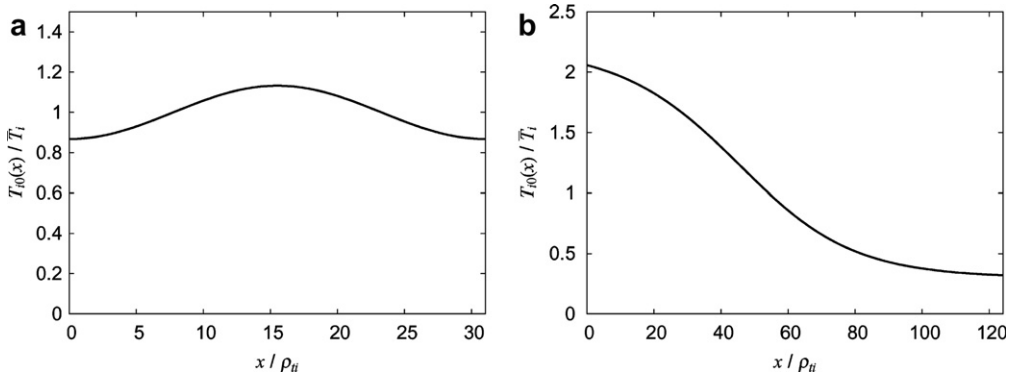

Fig. 2. The ion temperature profiles used in (a) 4D and (b) 5D ITG turbulence simulations.

smear out fine velocity space structures, the recurrence [41] is inevitable, and we thus stop the simulation before the recurrence occurs. Although the initial saturation amplitude is converged with much smaller $N_{v_\parallel}$, we use $N_{v_\parallel} = 128$ to keep an enough simulation time for studying numerical properties in the nonlinear phase. In a practical problem, $N_{v_\parallel}$ may be reduced by implementing a physical collision term, which possibly eliminates the recurrence.

Firstly, we discuss numerical properties of the skew-symmetric operator by comparing simulations with [Skew.] and with [Div.]. In the present ITG turbulence simulation, two ITG modes, which propagate

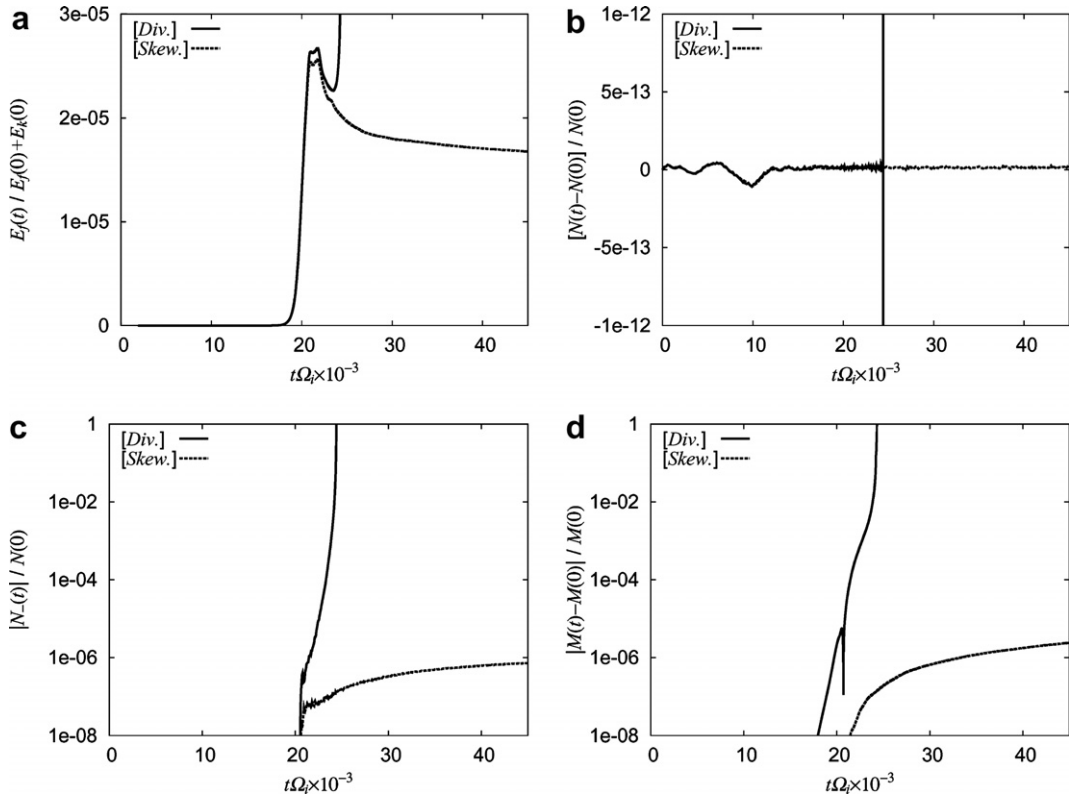

Fig. 3. The time histories of (a) the field energy, E_f, (b) the total particle number, N, (c) the negative particle number, N_-, and (d) the $L2$ norm, M, observed in ITG turbulence simulations with [Div.] and with [Skew.]. In (a), both simulations show almost the same saturation amplitudes, but the field energy in the simulation with [Div.] blows up at $t\Omega_i \times 10^{-3} \sim 24$. In (b), both simulations conserve N and show similar time histories until the simulation with [Div.] breaks down. In (c), the simulation with [Div.] shows a rapid growth of N_- which comes from numerical oscillations, while in the simulation with [Skew.], N_- is kept at a low level ($N_-/N(0) < 10^{-6}$). In (d), the simulation with [Div.] shows an exponential growth of the error of M, while the simulation with [Skew.] shows an approximate conservation of M.

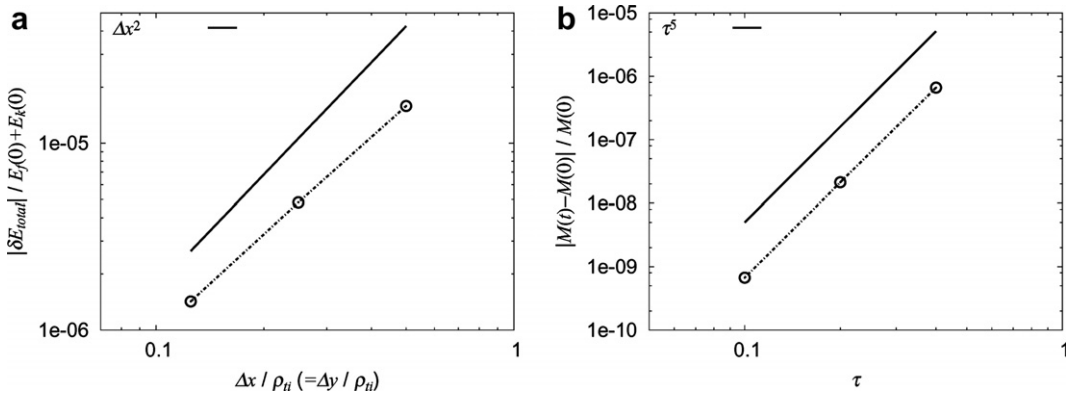

Fig. 4. The relative errors of (a) the total energy and (b) the $L2$ norm observed in the ITG turbulence simulation with the second order accurate skew-symmetric operator and the fourth order Runge–Kutta method. Values at $t\Omega_i \times 10^{-3} \sim 25$ are plotted against (a) $\Delta x(=\Delta y)$ and (b) the CFL number τ. The standard parameters are used except for these parameters. The errors of the total energy and the $L2$ norm increase with $|\delta E_{\text{total}}| \propto \Delta x^2$ and $|M(t) - M(0)| \propto \tau^5$, respectively.

in opposite directions, are excited in the positive and negative temperature gradient regions, respectively (see Fig. 5a). In the saturation phase, ITG modes saturate by self-generated zonal flows, which break up the linear mode structures. In the nonlinear phase, $m = n = 0$ zonal flows become dominant, and they are sustained almost in a quasi-steady level (see Fig. 5c), where $k_y = 2\pi m/L_y$ and $k_z = 2\pi n/L_z$. Fig. 3 shows the time evolutions of the field energy, E_{f}, the total particle number, N, the negative particle number, N_-, and the $L2$ norm, M, observed in these two simulations. Here, N_- is defined as the sum of spurious negative values of f over phase space. In Fig. 3a, the simulation with [Skew.] shows the nonlinear saturation, while the simulation with [Div.] breaks down in the saturation phase. In order to understand the cause of numerical instability, we check the conservations of N and M. As shown in Eqs. (30) and (34), [Div.] conserves only N. The simulation results in Figs. 3b and d also support this prediction. The exponential growth of the error of the $L2$ norm with a constant $L1$ norm leads to the growth of numerical oscillations, which produce spurious negative values of f. In Fig. 3c, a rapid growth of N_- is observed in the saturation phase. In contrast, [Skew.] conserves both the $L1$ and $L2$ norms, and the simulation with [Skew.] shows a conservation of N and an approximate conservation of M. Although spurious negative particles are produced also in the simulation with [Skew.], the growth of numerical oscillations or N_- is suppressed by the conservation of M, and the simulation is numerically stable for a long time in the nonlinear phase.

In Figs. 4a and b, the errors of the total energy and the $L2$ norm are checked by varying numerical parameters. In the present standard case, the error of the total energy is most sensitive to Δx and Δy, which determine resolution of the $E \times B$ nonlinearity. Although it is difficult to identify the cause of the error of the total energy, which is influenced also by a field solver, the error of the total energy increases with $\sim\Delta x^2$ in the convergence test in Fig. 4a. On the other hand, as discussed in the previous section, the error of M comes purely from the time integration error, which depends on the CFL number τ. In Fig. 4b, the error of the $L2$ norm is proportional to τ^5, which is consistent with the accuracy of the fourth-order Runge–Kutta method (with fifth-order accuracy [50]).

5. Comparisons between Vlasov and PIC simulations

In order to demonstrate the validity of the new Vlasov code, G5D, we show comparisons of ITG turbulence simulations using the Vlasov and PIC codes. A PIC simulation is performed using G3D [51], which was originally developed to study the slab electron temperature gradient driven (ETG) turbulence. In G3D, the gyrokinetic equation (2) is solved using the δf method, where the perturbed distribution function $\delta f = f - f_0$ is expressed by Monte-Carlo sampling via marker particles, and δf is solved along the nonlinear characteristics with an evolution equation of δf,

$$\frac{\mathrm{D}\delta f}{\mathrm{D}t} = -\{f_0, H\}, \tag{54}$$

or the constancy of f,

$$\delta f(\mathbf{Z}(t)) = f(\mathbf{Z}(t_0)) - f_0(\mathbf{Z}(t)). \tag{55}$$

In Ref. [52], it was shown that both methods give the same simulation results. Although a method to reduce a sampling noise was proposed [53], in this work, we use a conventional Maxwellian loading to make comparisons between cases with and without the $v_\parallel$ nonlinearity using the same initial marker particle distribution. In the initial condition, small particle weight is given for ion marker particles, and the initial perturbation (53) is given for the neutralising electron density. Since the initial particle weight is quickly damped after starting the simulation, the ITG mode grows from almost the same initial condition as the Vlasov simulation. In the 5D gyrokinetic simulation, the gyro-averaging is approximated by the four point sampling model which is valid for $k_\perp \rho_{\mathrm{ti}} \leqslant 2$ [54], while the reduced 4D simulation uses a guiding-centre model. The gyrokinetic Poisson equation is solved using a 2D finite element approximation with quadratic splines on the x–y plane and Fourier mode expansion in the z direction. Interactions between fields and particles are treated with the finite element PIC method [55]. In the finite element PIC method, subgrid scale noise is removed by basis functions of finite width, which act similarly to a shape factor of finite size particles in the ordinary PIC method [56–58]. In the z direction, we use a Gaussian shape factor. In Fourier space, these spline basis function and Gaussian shape factor work as a low-pass Fourier filter given as [56],

$$S(\mathbf{k}) = \left(\frac{\sin(k_x\delta x/2)}{k_x\delta x/2}\right)^3 \left(\frac{\sin(k_y\delta y/2)}{k_y\delta y/2}\right)^3 \exp\left(-\frac{k_z^2}{2\sigma_{k_z}^2}\right), \tag{56}$$

where δx and δy are the widths of spline basis functions in the x and y directions, respectively, and σ_{k_z} is the width of Gaussian shape factor. In order to make quantitative comparisons, in this section, we impose the Fourier filter (56) also to the Vlasov simulation. In the comparison, we use the fourth-order accurate skew-symmetric operator, which improves the quality of the total energy conservation.

5.1. 4D ITG Turbulence simulation

Firstly, we show comparisons of 4D ITG turbulence simulations with the standard case parameters. Numerical parameters of the PIC simulation are chosen from a convergence study, and we use 1.68×10^7 marker particles, $N_x \times N_y = 32 \times 16$ finite elements ($\delta x = \delta y \sim \rho_{\mathrm{ti}}$), $n = -6 \sim 6$, $\sigma_{k_z} = 7.5 \times 10^{-3}\rho_{\mathrm{ti}}^{-1}$, and $\Delta t = 20\Omega_i^{-1}$. This particle number corresponds to 2.52×10^3 particles per a finite element and a Fourier mode. Although the initial saturation amplitude is converged with much smaller particle number, we use this condition to see a long time behaviour of the PIC simulation. Numerical parameters of the Vlasov simulation are the same as the standard case except for $N_{v_\parallel} = 512$, which is also needed to have a long recurrence period in a long time simulation. By adding the Fourier filter, the linear growth rate and the initial saturation amplitude are reduced by ~4% and ~8%, respectively. The computational costs of the present 4D simulation are comparable between the Vlasov and PIC simulations, which require ~255 and ~211 processor × hours on the JAEA Altix3700Bx2 system, respectively.

In the linear phase, the most unstable mode is $n = m = 2$ mode, and its linear growth rate agrees well between the Vlasov ($\gamma \sim 1.235 \times 10^{-3}\Omega_i$) and PIC ($\gamma \sim 1.240 \times 10^{-3}\Omega_i$) simulations. In Fig. 5a, the linear eigenfunction also coincide with each other. In Figs. 5c and d, the time histories of the field energy, E_{f}, and the volume averaged ion thermal diffusivity, $\bar{\chi}_i$, are plotted. Although nonlinear transient behaviours for $t\Omega_i \times 10^{-3} = 25$–$30$ are slightly different, the initial ($t\Omega_i \times 10^{-3} \sim 22$) and quasi-steady ($t\Omega_i \times 10^{-3} \sim 45$) saturation levels show quantitative agreements between the Vlasov and PIC simulations. In Fig. 5b, nonlinear zonal flows also show almost the same structures. From these results, we conclude that the Vlasov and PIC codes give equivalent results at least up to the early nonlinear phase.

We then discuss about long time behaviours focusing on conservation properties. In the δf method, $N = \int f \, \mathrm{d}^6Z$ is conserved because the method is based on Eq. (55), but $\delta N = \int \delta f \, \mathrm{d}^6Z = -\int f_0 \, \mathrm{d}^6Z$, which

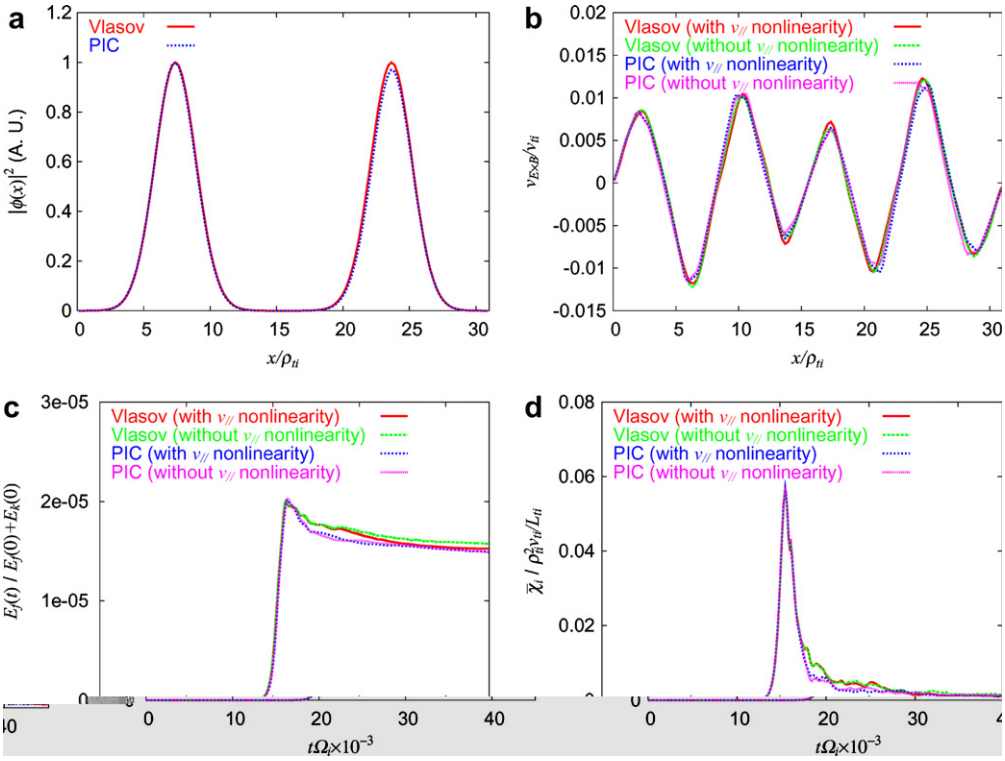

Fig. 5. Comparisons of 4D ITG turbulence simulations with and without the $v_{\parallel}$ nonlinearity. (a) shows the linear eigenfunction at $t\Omega_i \times 10^{-3} \sim 15$. Here, the linear eigenfunction exactly agrees between the cases with and without the $v_{\parallel}$ nonlinearity, and only the former case is plotted. (b) shows the structure of nonlinear zonal flows at $t\Omega_i \times 10^{-3} \sim 45$. (c) and (d) show the time histories of the field energy, E_f, and the volume averaged ion thermal diffusivity, $\bar{\chi}_i$, normalised with the gyro-Bohm coefficient, $\rho_{ti}^2 v_{ti}/L_{ti}$. All the comparisons show quantitative agreement among four cases.

is used in solving the electric field, is not conserved because of the statistical sampling error. This error may be further enhanced by errors in the nonlinear characteristics. The constancy of f along the nonlinear characteristics (55) is satisfied in an ideal system which is completely described by a single particle distribution function, f. However, in the δf PIC simulation, δf is expressed using a discrete Klimontovich distribution of weighted particles. Therefore, a solution of the gyrokinetic Poisson equation naturally involves a multiple particle correlation or a Coulomb collision, although it is suppressed in a quite low level by the Fourier filter (56). From the point of view of the entropy balance relation, the fluctuation entropy in a collisionless plasma increases monotonically in time, provided that quasi-steady heat transport is finite [18]. Accordingly, the particle weight, which is proportional to δf, also increases in time, and numerical collisions among weighted particles are enhanced as the particle weight becomes heavier. Because of numerical collisions, the nonlinear characteristics, $\mathbf{Z}(t)$, may be deviated from their true solution, $\mathbf{Z}_t(t)$, leading to the error of δf,

$$\delta f(\mathbf{Z}(t)) - \delta f(\mathbf{Z}_t(t)) = f_0(\mathbf{Z}_t(t)) - f_0(\mathbf{Z}(t)). \tag{57}$$

In addition, the numerical collision produces numerical heating. In Fig. 6, long time behaviours of the PIC and Vlasov simulations are compared. Although both simulations show an excellent total energy conservation in the early nonlinear phase, the total energy in the PIC simulation slowly increases in the nonlinear phase due to the numerical heating. It is noted that the rate of the numerical heating is not changed even with almost the same time step width as the Vlasov simulation, $\Delta t \sim 7\Omega_i^{-1}$. In contrast, the Vlasov simulation does not show such a numerical heating, and keeps a good energy conservation in a long time simulation. This is the most significant advantage of the new conservative gyrokinetic full-f Vlasov code. The error of the total energy in the Vlasov simulation is ~3% of the field energy after ~150 linear growth times.

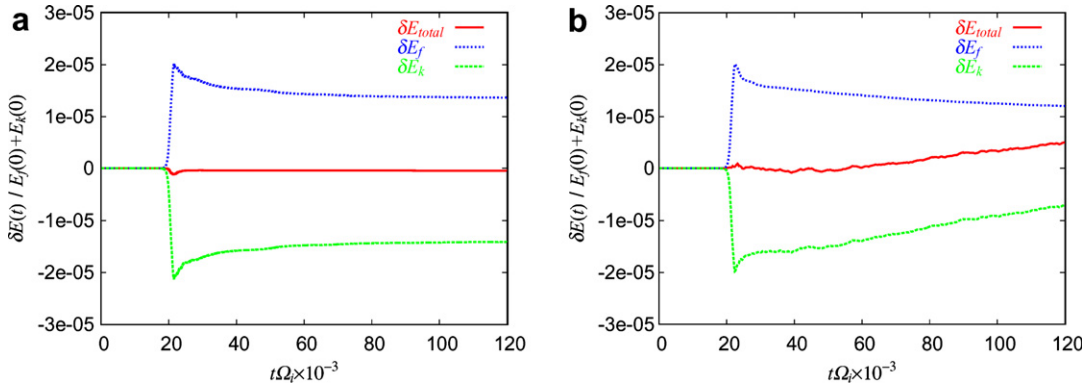

Fig. 6. The time histories of the total energy, δE_{total}, the field energy, δE_{f}, and the kinetic energy, δE_{k}, observed in long time ITG turbulence simulations using (a) the Vlasov code ($N_{v_\parallel} = 512$) and (b) the PIC code (1.67×10^7 marker particles). The PIC simulation shows monotonic increase of the total energy, while the total energy in the Vlasov simulation keeps almost constant. The error of the total energy at $t = 120 \times 10^3 \Omega_i^{-1} \sim 150\gamma^{-1}$ are ~3% and ~40% of the field energy in the Vlasov and PIC simulations, respectively.

5.2. Role of $v_\parallel$ nonlinearity

From the point of view of modern gyrokinetic theory, a gyrokinetic equation without the $v_\parallel$ nonlinearity, $\partial_z\phi\partial_{v_\parallel}\delta f$, is recognised as a conservative gyrokinetic equation with a spurious source term,

$$\frac{\mathrm{D}f}{\mathrm{D}t} = -\frac{q_i}{m_i}\frac{\partial\phi}{\partial z}\frac{\partial\delta f}{\partial v_\parallel}. \tag{58}$$

Here, we discuss how the spurious source term affects conservation properties. Firstly, it does not affect the total particle number conservation, because

$$\int \frac{q_i}{m_i}\frac{\partial\phi}{\partial z}\frac{\partial\delta f}{\partial v_\parallel}\,\mathrm{d}^6Z = 0. \tag{59}$$

On the other hand, the conservation of the $L2$ norm is violated by the spurious source term,

$$\int \frac{q_i}{m_i}\frac{\partial\phi}{\partial z} f\frac{\partial\delta f}{\partial v_\parallel}\,\mathrm{d}^6Z = \int \frac{q_i}{T_i}\frac{\partial\phi}{\partial z} v_\parallel \delta f f_0\,\mathrm{d}^6Z \neq 0. \tag{60}$$

In the PIC simulation, Eq. (59) may not be satisfied because of the statistical sampling error. In addition, the PIC simulation without the $v_\parallel$ nonlinearity uses Eq. (54) or (55) with the partially linearised characteristics given by $\mathrm{d}\mathbf{R}/\mathrm{d}t = v_\parallel\mathbf{b} + c/B_0\mathbf{b}\times\nabla\phi$ and $\mathrm{d}v_\parallel/\mathrm{d}t = 0$, which may lead to similar errors as in Eq. (57). In Fig. 7a, the particle number conservation becomes worse without the $v_\parallel$ nonlinearity. However, the error of the particle number, δN, is still at the same order as the inherent error in the PIC simulation, and its effect on the saturation level is quite small as shown in Figs. 5c and d. On the other hand, in the Vlasov simulation, the conservation of the $L2$ norm is violated if the $v_\parallel$ nonlinearity is neglected, although the total particle number is exactly conserved even without the $v_\parallel$ nonlinearity. In Fig. 7b, the error of the $L2$ norm in the initial saturation phase shows different behaviours between the cases with and without the $v_\parallel$ nonlinearity. But, in the nonlinear phase, their behaviours are very similar, because zonal flows, which are not subject to the $v_\parallel$ nonlinearity, become dominant. The errors of the $L2$ norm in these two cases are of the same order, and the saturation levels in Figs. 5c and d are almost the same.

From the point of view of a physical effect, the influence of the $v_\parallel$ nonlinearity on heat transport can be seen by considering the entropy balance relation. The entropy balance relation is derived by multiplying $\delta f/f_0$ to Eq. (14) and integrating it over phase space,

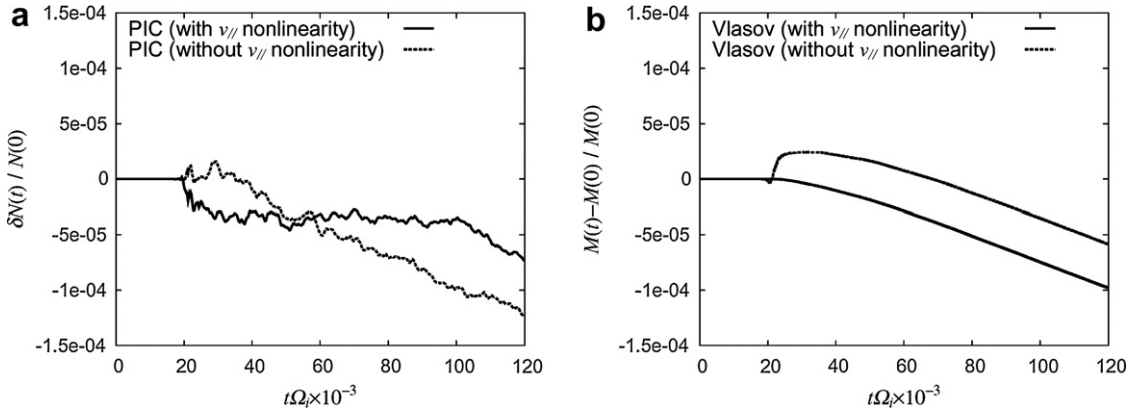

Fig. 7. The errors of (a) the particle number δN in the PIC simulation and (b) the $L2$ norm in the Vlasov simulation are compared between the cases with and without the $v_\parallel$ nonlinearity. In the Vlasov code, the total particle number is exactly conserved in both cases.

$$\frac{\mathrm{d}\delta S}{\mathrm{d}t} + D_{E\times B} + D_{v_\parallel} + D_{\mathrm{flux}} + D_{\mathrm{field}} = 0, \tag{61}$$

$$D_{E\times B} = \int \frac{c}{B_0}\mathbf{b}\times\nabla\phi\cdot\nabla\ln f_0\left(\frac{\delta f^2}{2f_0}\right)\mathrm{d}^4Z, \tag{62}$$

$$D_{v_\parallel} = \int \frac{q_i}{T_i}\frac{\partial\phi}{\partial z}v_\parallel\left(\frac{\delta f^2}{2f_0}\right)\mathrm{d}^4Z, \tag{63}$$

$$D_{\mathrm{flux}} = \int \frac{c}{B_0}\mathbf{b}\times\nabla\phi\cdot\nabla\ln f_0\delta f\ \mathrm{d}^4Z, \tag{64}$$

$$D_{\mathrm{field}} = \int \frac{q_i}{T_i}\frac{\partial\phi}{\partial z}v_\parallel\delta f\ \mathrm{d}^4Z, \tag{65}$$

where $\mathrm{d}^4Z = m_i\,\mathrm{d}\mathbf{R}\,\mathrm{d}v_\parallel$ and the fluctuation entropy is defined as $\delta S \equiv \int \delta f^2/2f_0\,\mathrm{d}^4Z$. The fluctuation entropy means a difference between microscopic and macroscopic entropy, $\delta S = \int f\ln f\,\mathrm{d}^4Z - \int f_0\ln f_0\,\mathrm{d}^4Z + \mathcal{O}(\delta f^3)$ [18]. The entropy balance relation (61) is derived for the present global model where equilibrium quantities and their gradients vary consistently. In the limit of a local approximation with constant T_i and ∇T_i or a complete scale separation between equilibrium and fluctuating quantities, $D_{E\times B}$, D_{flux}, and D_{field} reduce to

$$D_{E\times B} = 0, \tag{66}$$

$$D_{\mathrm{flux}} = \frac{n_0}{2T_i}\left[\int \frac{c}{B_0}\mathbf{b}\times\nabla\phi\delta T_i\,\mathrm{d}\mathbf{R}\right]\cdot\nabla\ln T_i, \tag{67}$$

$$D_{\mathrm{field}} = \frac{1}{T_i}\frac{\mathrm{d}E_{\mathrm{f}}}{\mathrm{d}t}, \tag{68}$$

where $\delta T_i \equiv \int(m_i v_\parallel^2)\delta f m_i\,\mathrm{d}v_\parallel/n_0$. In Fig. 8a, the terms in the entropy balance relation (61) are plotted. It is shown that the heat transport, D_{flux}, is balanced mainly with the entropy production, $\mathrm{d}\delta S/\mathrm{d}t$, and in the quasi-steady phase, a steady solution with $D_{\mathrm{flux}} \sim 0$ is realized. This result is consistent with results obtained in a local model without the $v_\parallel$ nonlinearity [18]. In the present study, it is confirmed that even though the $v_\parallel$ nonlinearity is kept, its contribution to the entropy balance relation is almost negligible.

5.3. 5D ITG turbulence simulation

In 5D ITG turbulence simulations, we consider a hydrogen plasma in a slab configuration with $L_x = 4L_y \sim 124\rho_{\mathrm{ti}}$, $L_z \sim 8000\rho_{\mathrm{ti}}$, $L_{v_\parallel} = 10v_{\mathrm{ti}}$ ($v_\parallel = -5v_{\mathrm{ti}} \sim 5v_{\mathrm{ti}}$), and $L_{v_\perp} = 3.5v_{\mathrm{ti}}$ ($|v_\perp| = 0$–$3.5v_{\mathrm{ti}}$). n_0 and T_{e0} are uniform, and T_{i0} is given as

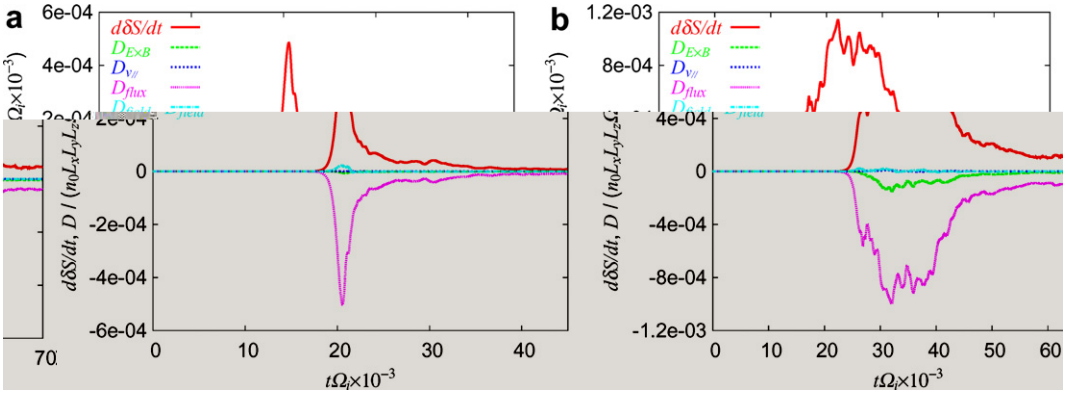

Fig. 8. The time histories of terms in the entropy balance relation observed in (a) 4D and (b) 5D ITG turbulence simulations using the Vlasov code. The errors in the entropy balance relation are (a) $\sim 1.5 \times 10^{-6}$ at $t = 120 \times 10^3 \Omega_i^{-1}$ and (b) $\sim 8 \times 10^{-6}$ at $t = 70 \times 10^3 \Omega_i^{-1}$. The heat flux, D_{flux}, is balanced with the entropy production, $\mathrm{d}\delta S/\mathrm{d}t$, in both cases. The maximum values of the contribution from the $v_\parallel$ nonlinearity, $D_{v_\parallel}$, are (a) $\sim$0.3% and (b) $\sim$0.9% of $\mathrm{d}\delta S/\mathrm{d}t$, respectively.

$$T_{i0}(x) = \bar{T}_i \exp\left(-\frac{\Delta r}{L_{\text{ti}}} \tanh \frac{x - L_x/2}{\Delta r}\right), \tag{69}$$

where $L_{\text{ti}} = \Delta r = 0.3 L_x$ and $\int T_{i0}\, \mathrm{d}x/L_x = T_{e0}$ (see Fig. 2b). These parameters are similar to those used in cylindrical ITG turbulence simulations in Ref. [46]. In the present case, we impose a fixed boundary condition in the x direction in the same manner as in the $v_\parallel$ direction, $\bar{v}_1^{1x_1} = 0$. The gyrokinetic Poisson equation (8) is also solved with a fixed boundary condition, $\phi = 0$, at $x = 0$, L_x. From a convergence study, we choose numerical parameters of the Vlasov simulation as $N_x \times N_y \times N_z \times N_{v_\parallel} \times N_{v_\perp} = 256 \times 64 \times 32 \times 192 \times 16$ and $\tau = 0.4$, which corresponds to $\Delta t \sim 20\Omega_i^{-1}$ and $\Delta t \sim 4\Omega_i^{-1}$ in the linear and nonlinear phase. Here, the 5D Vlasov simulation is converged with larger grid width ($\Delta x = \Delta y \sim \rho_{\text{ti}}/2$) than the 4D simulation, because of the FLR effect. In the PIC simulation, we use the same numerical parameters except for 6.71×10^7 marker particles, and $N_x \times N_y = 128 \times 32$ finite elements. In the 5D benchmark, the computational costs and the memory usage of the Vlasov and PIC simulations are, respectively, $\sim$2100 and $\sim$3800 processor $\times$ hours, and $\sim$100 GB and $\sim$20 GB on the JAEA Altix3700Bx2 system.

Although the linear eigenfunctions of the most unstable mode with $n = 2$, $m = 3$ agree well with each other in Fig. 9a, the linear growth rate observed in the PIC simulation ($\gamma \sim 0.857 \times 10^{-3} \Omega_i$) is slightly lower ($\sim$2%) than that in the Vlasov simulation ($\gamma \sim 0.873 \times 10^{-3} \Omega_i$), because the gyro-averaging is calculated using different models, $J_0(k_\perp \rho)$ in the Vlasov simulation and the four point sampling model in the PIC simulation. The time histories of the field energy, E_{f}, and the volume averaged ion thermal diffusivity, $\bar{\chi}_i$, are shown in Figs. 9c and d. After the saturation of the most unstable mode at $t\Omega_i \times 10^{-3} \sim 28$, a turbulent region spreads towards boundaries in the nonlinear evolution phase for $t\Omega_i \times 10^{-3} = 30$–$50$, and then, the system goes to the quasi-steady phase dominated by zonal flows. Although the saturation levels of E_{f} and $\bar{\chi}_i$ show reasonably good agreements between the Vlasov and PIC simulations, the quantitative agreements are not so good as 4D simulations, because of slightly different linear growth rates and complicated turbulence spreading processes in the nonlinear evolution phase. In Fig. 9b, zonal flows apart from the most unstable region at $x = L_x/2$ are produced through the nonlinear turbulence spreading processes, and their structures show different patterns. It should be noted that in the PIC simulation, the zonal flows or the radial electric fields are not zero at the boundaries because of the error of the particle number. The breakdown of the total energy conservation at $t\Omega_i \times 10^{-3} = 70$ is $\sim$10% and $\sim$22% of the field energy in the Vlasov and PIC simulations, respectively.

Effects of the $v_\parallel$ nonlinearity are investigated also in 5D ITG simulations. In the entropy balance relation in Fig. 8b, the contribution from the $v_\parallel$ nonlinearity is negligible. Here, the entropy balance relation can be derived also for the 5D gyrokinetic model in the similar way as in the 4D reduced model. However, in Fig. 9, differences between the cases with and without the $v_\parallel$ nonlinearity are enhanced compared to those in the 4D ITG simulations. The errors of the particle number in the PIC simulation and of the $L2$ norm in

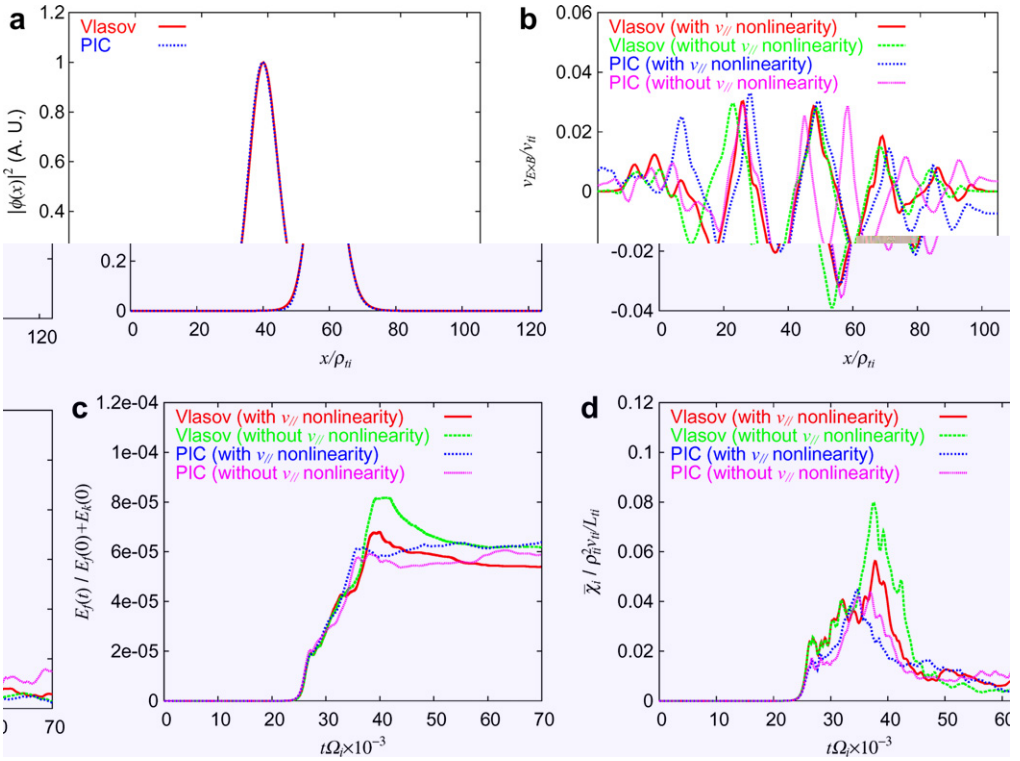

Fig. 9. Comparisons of 5D ITG turbulence simulations with and without the $v_{\parallel}$ nonlinearity. Plots are the same as Fig. 5. In (a) and (b), the linear eigenfunction and the zonal flow structure are observed at $t\Omega_i \times 10^{-3} \sim 20$ and $t\Omega_i \times 10^{-3} \sim 70$.

the Vlasov simulation are shown in Figs. 10a and b. In contrast to the 4D simulations, in which an influence of the $v_{\parallel}$ nonlinearity on these errors appears only in the initial saturation phase, the errors in the 5D simulations are continuously produced by turbulent activities with finite $\partial\phi/\partial z$ in the nonlinear evolution phase. Especially, in the Vlasov simulation, the error of the $L2$ norm in the case without the $v_{\parallel}$ nonlinearity becomes an order of magnitude larger than the inherent error due to the time integration scheme. These results show that the $v_{\parallel}$ nonlinearity is physically unimportant, but may produce significant errors numerically.

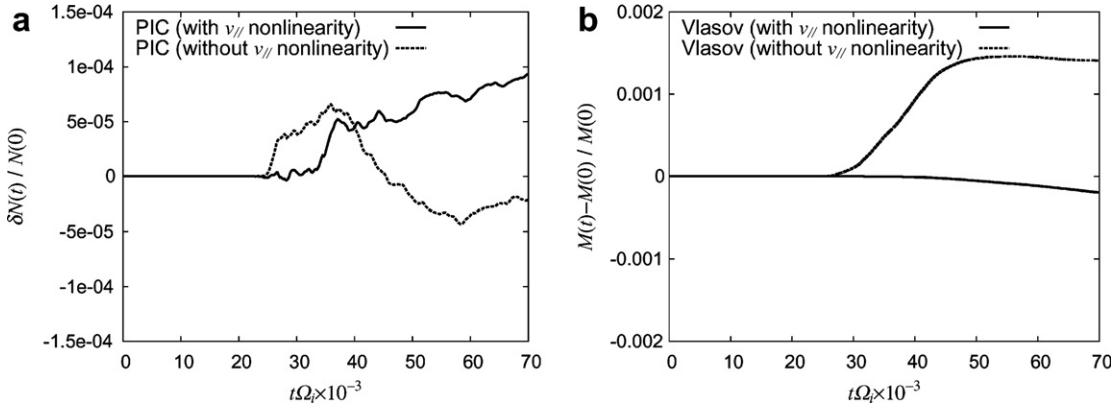

Fig. 10. The errors of (a) the particle number δN in the PIC simulation and (b) the $L2$ norm in the Vlasov simulation are compared between 5D ITG simulations with and without the $v_{\parallel}$ nonlinearity. In the Vlasov code, the total particle number is exactly conserved in both cases.

6. Summary

In this work, we have developed a new conservative gyrokinetic full-f Vlasov code, G5D, using the Morinishi scheme. In the scheme, the skew-symmetric finite difference operator conserves both the $L1$ and $L2$ norms. Numerical properties of the new Vlasov code have been discussed by comparing the results from ITG turbulence simulations with the skew-symmetric operator and with the divergence operator. Here, the latter scheme is equivalent to a finite volume method or a centred finite difference method. The comparison has shown that the former scheme is numerically stable and robust in a long time simulation, while the simulation with the latter scheme breaks down in the nonlinear phase. The ITG simulation with the skew-symmetric operator shows an exact conservation of the $L1$ norm and an approximate conservation of the $L2$ norm. Here, the small error of the $L2$ norm comes not from the nonlinear convection term but from the time integration scheme. From these results, it has been demonstrated that the conservation of the $L2$ norm is very helpful for avoiding the growth of numerical oscillations. In addition to the conservations of the $L1$ and $L2$ norms, the total energy conservation is confirmed. Although small spurious negative values of f, which violate the definition of the kinetic entropy, are observed, the simulation satisfies the entropy balance relation of the fluctuation entropy, which is much more relevant in dictating the turbulent heat flux.

The new Vlasov code has been successfully benchmarked against a conventional δf PIC code, G3D. ITG turbulence simulations with the Vlasov and PIC codes show reasonably good agreement both in the linear and early nonlinear phases. In a long time simulation, the new Vlasov code shows the good total energy conservation as well as the exact particle number conservation, while in the PIC simulation, the particle number is not conserved and the total energy slowly increases due to the numerical heating. Conservations of the total particle number and the total energy are essential properties for a long time full-f Vlasov simulation with evolving background profiles. The results show that the new conservative gyrokinetic full-f Vlasov code satisfies these requirements. In the present benchmark parameters, the computational cost of the Vlasov simulation is comparable to that of the PIC simulation, although the memory usage of the Vlasov simulation is larger by $\sim$5 times.

The effect of the $v_\parallel$ nonlinearity has been clarified both in the Vlasov and PIC simulations. The entropy balance relation shows that the contribution from the $v_\parallel$ nonlinearity is physically unimportant. However, comparisons between the simulations with and without the $v_\parallel$ nonlinearity have shown that it affects conservation properties numerically. The simulation without the $v_\parallel$ nonlinearity produces the error of the particle number in the PIC simulation, while it leads to the error of the $L2$ norm in the Vlasov simulation.

In the present decaying turbulence simulation, the influence from the absence of the $v_\parallel$ nonlinearity is very limited, because the quasi-steady phase is dominated by zonal flows which are not subject to the $v_\parallel$ nonlinearity. However, in driven turbulence simulations, the error of the $L2$ norm may be further enhanced by continuously driven turbulent activities with finite parallel electric fields. In this work, it has been shown that the conservation of the $L2$ norm is important for numerical stability. In addition, in a toroidal geometry, the phase space conservation law [59] is not satisfied without the $v_\parallel$ nonlinearity, because $\partial(B^*_\parallel \dot{v}_{\parallel 1})/\partial v_\parallel \neq 0$, where $B^*_\parallel = \mathbf{b}\cdot[\mathbf{B} + (B_0/\Omega_i)\nabla\times\mathbf{b}v_\parallel]$ and $\dot{v}_{\parallel 1}$ is a perturbed part of nonlinear characteristics in $v_\parallel$. Obviously, this violates the total particle number conservation. In Ref. [60], comparisons of toroidal δf simulations with and without the $v_\parallel$ nonlinearity were shown, and it was reported that its effect was unimportant for their δf simulations with fixed background profiles. However, it is not so clear how the breakdown of conservation properties affects long time behaviours of full-f simulations with evolving background profiles, because spurious electromagnetic fields and background profiles may build up due to accumulation of such errors. In future works, the code will be extended to a toroidal geometry, and non-conservative effects will also be implemented towards a long time driven turbulence simulation. And, the above issue will be addressed again.

Acknowledgments

One of the authors (Y.I.) thanks Drs. T.-H. Watanabe and H. Sugama for stimulating discussions on the non-dissipative Vlasov simulation and the entropy balance relation, and two of the authors (Y.I. and L.V.) are grateful to Drs. M. Brunetti, S. Brunner, V. Grandgirard, and R. Hatzky for useful discussions on the semi-Lagrangian Vlasov simulation and the δf PIC simulation. The authors thank Drs. M. Kikuchi, T. Hirayama,

M. Azumi, and K. Appert for their support. The simulations were performed on the JAEA Altix3700Bx2 system. This work is supported by the Japanese Ministry of Education, Culture, Sports, Science, and Technology, Grant Nos. 18760647 and 17760151, and partly by the Swiss National Science Foundation.

References

[1] L. Villard et al., First principle based simulations of instabilities and turbulence, Plasma Phys. Control. Fusion 46 (2004) B51.
[2] W.M. Tang, V.S. Chan, Advances and challenges in computational plasma science, Plasma Phys. Control. Fusion 47 (2005) R1.
[3] Y. Idomura, T.-H. Watanabe, H. Sugama, Kinetic simulations of turbulent fusion plasmas, C. R. Phys. 7 (2006) 650.
[4] S.E. Parker, W.W. Lee, R.A. Santoro, Gyrokinetic simulation of ion temperature gradient driven turbulence in 3D toroidal geometry, Phys. Rev. Lett. 71 (1993) 2042.
[5] Y. Kishimoto et al., Self-organized critical gradient transport and shear flow effects for ion temperature gradient mode in toroidal plasmas, in: Proceedings of the 15th International Conference on Plasma Physics and Controlled Nuclear Fusion research, IAEA, Vienna, 1994.
[6] R.D. Sydora, V.K. Decyk, J.M. Dawson, Fluctuation-induced heat transport results from a large global 3D toroidal particle simulation model, Plasma Phys. Control. Fusion 38 (1996) A281.
[7] T.M. Tran et al., Global gyrokinetic simulation of ion temperature gradient driven instabilities using particles, in: Theory of Fusion Plasmas, Int. Workshop, 1999, p. 45.
[8] Y. Idomura, S. Tokuda, Y. Kishimoto, Global gyrokinetic simulation of ion temperature gradient driven turbulence in plasmas using a canonical Maxwellian distribution, Nucl. Fusion 43 (2003) 234.
[9] M. Kotschenreuther et al., Novel computational techniques to predict transport in confinement devices, and applications to ion temperature gradient driven turbulence, in: Proceedings of the 13th International Conference on Plasma Physics and Controlled Nuclear Fusion Research, IAEA, Vienna, 1990.
[10] S.E. Parker, W.W. Lee, A fully nonlinear characteristic method for gyrokinetic simulation, Phys. Fluids B 5 (1993) 77.
[11] A.Y. Aydemir, A unified Monte Carlo interpretation of particle simulation and applications to non-neutral plasmas, Phys. Plasmas 1 (1994) 822.
[12] Y. Idomura, S. Tokuda, Y. Kishimoto, Global profile effects and structure formations in toroidal electron temperature gradient driven turbulence, Nucl. Fusion 45 (2005) 1571.
[13] Y. Idomura, Self-organization in electron temperature gradient driven turbulence, Phys. Plasmas 13 (2006) 080701.
[14] P. Angelino et al., Effects of plasma current on nonlinear interactions of ITG turbulence, zonal flows and geodesic acoustic modes, Plasma Phys. Control. Fusion 48 (2006) 557.
[15] W.W. Lee, W.M. Tang, Gyrokinetic particle simulation of ion temperature gradient drift instabilities, Phys. Fluids 31 (1988) 612.
[16] J.A. Krommes, G. Hu, The role of dissipation in the theory and simulations of homogeneous plasma turbulence, and resolution of the entropy paradox, Phys. Plasmas 1 (1994) 3211.
[17] H. Sugama et al., Transport processes and entropy production in toroidal plasmas with gyrokinetic electromagnetic turbulence, Phys. Plasmas 3 (1996) 2379.
[18] T.-H. Watanabe, H. Sugama, Kinetic simulation of a quasisteady state in collisionless ion temperature gradient driven turbulence, Phys. Plasmas 9 (2002) 3659.
[19] A.M. Dimits et al., Scalings of ion-temperature-gradient-driven anomalous transport in tokamaks, Phys. Rev. Lett. 77 (1996) 71.
[20] Z. Lin, T.S. Hahm, Turbulence spreading and transport scaling in global gyrokinetic particle simulation, Phys. Plasmas 11 (2004) 1099.
[21] Z. Lin et al., Effects of collisional zonal flow damping on turbulent transport, Phys. Rev. Lett. 83 (1999) 3645.
[22] S. Brunner, E. Valeo, J.K. Krommes, Collisional delta-f scheme with evolving background for transport time scale simulations, Phys. Plasmas 6 (1999) 4504.
[23] W.X. Wang et al., A new δf method for neoclassical transport studies, Plasma Phys. Control. Fusion 41 (1999) 1091.
[24] S. Satake et al., Non-local neoclassical transport simulation of geodesic acoustic mode, Nucl. Fusion 45 (2005) 1362.
[25] W. Dorland et al., Gyrokinetic simulations of tokamak microturbulence, in: Proceedings of the 18th IAEA Fusion Energy Conference, IAEA, Vienna, 2000.
[26] F. Jenko, Massively parallel Vlasov simulation of electromagnetic drift-wave turbulence, Comput. Phys. Commun. 125 (2000) 196.
[27] T.H. Watanabe, H. Sugama, Velocity-space structures of distribution function in toroidal ion temperature gradient turbulence, Nucl. Fusion 46 (2006) 24.
[28] J. Candy, R. Waltz, An Eulerian gyrokinetic-Maxwell solver, J. Comput. Phys. 186 (2003) 545.
[29] P.A. Politzer, Observation of avalanchelike phenomena in a magnetically confined plasma, Phys. Rev. Lett. 84 (2000) 1192.
[30] H. Takenaga et al., Temporal variation of density fluctuation and transport in reversed shear plasmas on JT-60U, Plasma Phys. Control. Fusion 48 (2006) A401.
[31] X. Garbet et al., Flux driven turbulence in tokamaks, Nucl. Fusion 39 (1999) 2063.
[32] S. Benkadda et al., Bursty transport in tokamak turbulence: role of zonal flows and internal transport barriers, Nucl. Fusion 41 (2001) 995.
[33] M. Brunetti et al., A semi-Lagrangian code for nonlinear global simulations of electrostatic drift-kinetic ITG modes, Comput. Phys. Commun. 163 (2004) 1.
[34] V. Grandgirard et al., A drift-kinetic semi-Lagrangian 4D code for ion turbulence simulation, J. Comput. Phys 217 (2006) 395.

[35] Y. Idomura, Y. Kishimoto, S. Tokuda, Comparisons of gyrokinetic PIC and CIP codes, in: 32nd EPS Conference on Plasma Physics, P-1.044, 2005.
[36] E. Sonnendrücker et al., The semi-Lagrangian method for the numerical resolution of the Vlasov equation, J. Comput. Phys. 149 (1999) 201.
[37] T. Nakamura, T. Yabe, Cubic interpolated propagation scheme for solving the hyper-dimensional Vlasov–Poisson equation in phase space, Comput. Phys. Commun. 120 (1999) 122.
[38] F. Filbet, E. Sonnendrücker, P. Bertrand, Conservative numerical schemes for the Vlasov equation, J. Comput. Phys. 172 (2001) 166.
[39] F. Xiao et al., Conservative and oscillation-less atmospheric transport schemes based on rational functions, J. Geophys. Res. 107 (2002) 4609.
[40] M. Ida, A conservative semi-Lagrangian method for oscillation-free computation of advection processes, Comput. Phys. Commun. 143 (2002) 142.
[41] C.Z. Cheng, G. Knorr, The integration of the Vlasov equation in configuration space, J. Comput. Phys. 22 (1976) 330.
[42] A. Arakawa, Computational design for long-term numerical integration of the equations of fluid motion: two-dimensional incompressible flow. Part I, J. Comput. Phys. 1 (1966) 119.
[43] Y. Morinishi et al., Fully conservative higher order finite difference schemes for incompressible flow, J. Comput. Phys. 143 (1998) 90.
[44] T.-H. Watanabe, H. Sugama, T. Sato, A nondissipative simulation method for the drift kinetic equation, J. Phys. Soc. Japan 70 (2001) 3565.
[45] E.A. Frieman, L. Chen, Nonlinear gyrokinetic equation for low-frequency electromagnetic waves in general plasma equilibria, Phys. Fluids 25 (1982) 502.
[46] L. Villard et al., Full radius linear and nonlinear gyrokinetic simulations for tokamaks and stellarators: zonal flows, applied $E \times B$ flows, trapped electrons and finite beta, Nucl. Fusion 44 (2004) 172.
[47] T.S. Hahm, Nonlinear gyrokinetic equations for tokamak microturbulence, Phys. Fluids 31 (1988) 2670.
[48] J.M. Sanz-Serna, Symplectic Runge–Kutta and related methods: recent results, Physica D 60 (1992) 293.
[49] J. de Frutos, J.M. Sanz-Serna, An easily implementable fourth-order method for the time integration of wave problems, J. Comput. Phys. 103 (1992) 160.
[50] W.H. Press et al., Numerical Recipes in Fortran77, Cambridge University Press, New York, 1986.
[51] Y. Idomura, M. Wakatani, S. Tokuda, Stability of $E \times B$ zonal flow in electron temperature gradient driven turbulence, Phys. Plasmas 7 (2000) 3551.
[52] S.J. Allfrey, R. Hatzky, A revised δf algorithm for nonlinear PIC simulation, Comput. Phys. Commun. 154 (2003) 98.
[53] R. Hatzky et al., Energy conservation in a nonlinear gyrokinetic particle-in-cell code for ion-temperature-gradient-driven modes in θ-pinch geometry, Phys. Plasmas 9 (2002) 898.
[54] W.W. Lee, Gyrokinetic particle simulation model, J. Comput. Phys. 72 (1987) 243.
[55] M. Fivaz et al., Finite element approach to global gyrokinetic particle-in-cell simulations using magnetic coordinates, Comput. Phys. Commun. 111 (1998) 27.
[56] C.K. Birdsall, A.B. Langdon, Plasma Physics via Computer Simulation, Adam Hilger, Bristol and New York, 1991.
[57] R.W. Hockney, J.W. Eastwood, Computer Simulation Using Particles, Adam Hilger, Bristol and New York, 1988.
[58] T. Tajima, Computational Plasma Physics: With Applications to Fusion and Astrophysics, Addison-Wesley, Redwood City, CA, 1989.
[59] A.J. Brizard, Nonlinear gyrokinetic Vlasov equation for toroidally rotating axisymmetric tokamaks, Phys. Plasmas 2 (1995) 459.
[60] J. Candy et al., Relevance of the parallel nonlinearity in gyrokinetic simulations of tokamak plasmas, Phys. Plasmas 13 (2006) 074501.